THE JOURNAL OF PHYSICAL CHEMISTRY B

Article

pubs.acs.org/JPCB

Accommodation of a Central Arginine in a Transmembrane Peptide by Changing the Placement of Anchor Residues

Vitaly V. Vostrikov,[†] Benjamin A. Hall,[‡] Mark S. P. Sansom,[‡] and Roger E. Koeppe, II*,[†]

[†]Department of Chemistry and Biochemistry, University of Arkansas, Fayetteville, Arkansas 72701, United States

[‡]Department of Biochemistry & Oxford Centre for Integrative Systems Biology, University of Oxford, South Parks Road, Oxford, OX1 3QU, United Kingdom

Supporting Information

ABSTRACT: Both Trp and Arg in transmembrane protein domains make important interactions with lipids at the membrane/water interface, but at different depths. Derivatives of the designed peptide GWALP23, acetyl-GGALW^{5}LALALALALALALW^{19}LAGA-amide, with single Trp anchors, have proven useful for characterizing such interactions. Indeed, previous work revealed quite different effects emanating from Arg substitutions at positions 12 and 14 within GWALP23, with the R12 peptide exhibiting multiple positions and orientations with respect to DOPC bilayer membranes (Vostrikov et al. *J. Am. Chem. Soc.* **2010**, *132*, 5803−5811). To gain further understanding of the multistate behavior, we moved the Trp "anchor" residues to more outer positions 3 and 21 in GWALP23 itself, and in the R12 and R14 derivatives. The locations and orientations of the peptides with respect to lipid bilayer membranes of differing thickness were investigated by means of solid-state ^{2}H NMR spectroscopy, using labeled alanines, and coarse-grained molecular dynamics simulations. Interestingly, relatively intense and narrow ^{2}H resonances from selected backbone C_α deuterons were observed over quite narrow ranges of frequency and sample orientation. The backbone resonances reflect dynamic complexities and at the same time provide important contributions for the analysis of peptide transmembrane orientation. With the Trp^{3,21} anchors relatively far from the peptide and bilayer center, the results indicate significantly large apparent tilt angles, for example, close to 30° for the new R12 and R14 peptides with respect to the bilayer normal of DLPC membranes. The R12 side chain indeed is "rescued" to a stable position, where it is accommodated within the transmembrane helix, when the Trp anchors are moved outward and to another face of the helix. At the same time, the R14 side chain of transmembrane GW^{3,21}ALP23 also retains a stable favored position.

1. INTRODUCTION

Ionizable amino acid residues usually are poorly tolerated in nonpolar surroundings, whether the hydrophobic core of a protein or the acyl-chain interior of a lipid bilayer. In cases where charged residues are present in such environments, the residues often are highly conserved and essential for protein function. The "buried" charged side chains also may be stabilized by formidable networks of protein−protein interactions.[1,2] In other cases, the presence of polar or charged residues in unfavorable, hydrophobic regions can have detrimental consequences for protein stability and/or function.[3,4] Furthermore, many of the permissible mutations that place an ionizable residue in the hydrophobic core of a protein are accompanied by pK_a shifts, which render the side chain noncharged.[5,6] In similar fashion, burying a polar amino acid in the hydrophobic interior of a lipid bilayer membrane can be challenging. Selected examples do exist, nevertheless, such as the voltage-sensing S4 domains that regulate particular cation channels by means of multiple Arg residues; yet their accommodation in the membrane could involve extensive charge compensation.[7]

Numerous investigations have addressed the question: How difficult is it to incorporate an uncompensated charged residue in a lipid bilayer membrane?[8−10] While an ultimate goal is the discovery of principles or "rules" that govern the behavior of transmembrane proteins, many intermediate goals call for the testing of specific hypotheses. For example, a profound effect of charge state on membrane insertion has been demonstrated for the case of an isolated α-helix with four histidine residues. At high pH, such a model peptide was capable of spanning the membrane, but His protonation under acidic conditions caused an alteration of peptide topography and resulted in its exclusion from the lipid bilayer.[11,12] Such pH-dependent behavior is manifest for acidic as well as basic ionizable residues, for example, by a sequence derived from bacteriorhodopsin, termed pH low insertion peptide (pHLip), which contains Asp residues within a hydrophobic stretch; when protonated at low pH, these peptides incorporate into lipid bilayer membranes.[13,14]

Another important factor is the sequence position of a charged residue. A comprehensive study of translocon-mediated insertion of α-helices coupled with a glycosylation

Received: August 16, 2012
Revised: October 2, 2012
Published: October 2, 2012

assay led to Gaussian free energy profiles for the charged residues, with maxima close to the bilayer center.[8] Hydrophilic amino acids with flexible side chains nevertheless are capable of "snorkeling" toward the more polar membrane−water interfaces, thus allowing such residues to "bridge" nonpolar and polar environments. Additionally, an entire peptide or domain may be "lifted" toward the interface of one leaflet to satisfy some of the polarity preferences.[15,16]

Previously, we examined a single arginine incorporated near the center of GWALP23 (GGALW^5[LA]$_6$LW^{19}LAGA), a designed transmembrane peptide derived from the "WALP" family[17,18] but importantly having only one Trp residue flanking each end of a hydrophobic [LA]$_{6.5}$ core helix. Two peptides having identical amino acid composition and a single Arg residue at either position 12 or position 14 within GWALP23 (Table 1) display markedly different behavior.

Table 1. Peptide Sequences for GWALP23 and Derivatives[a]

peptide	sequence
GW^{5,19}ALP23	GGALWLALALALALALALWLAGA
GW^{5,19}ALP23-R12	GGALWLALALARALALALWLAGA
GW^{5,19}ALP23-R14	GGALWLALALALARALALWLAGA
GW^{3,21}ALP23	GGWLALALALALALALALALWGA
GW^{3,21}ALP23-R12	GGWLALALALARALALALALWGA
GW^{3,21}ALP23-R14	GGWLALALALALARALALALWGA

[a]Sequence positions 12 and 14 are underlined, for emphasis. The parent GWALP23 sequence includes tryptophans (**W**) at positions 5 and 19. The termini of all peptides are blocked with *N*-acetyl and either *C*-amide or *C*-ethanolamide.

While GWALP23-R14 adopts a transmembrane orientation, the R12 sequence isomer populates both transmembrane and interfacial states in DOPC.[16] The position of the single arginine, relative to the two tryptophans, is different on a helical wheel projection of GWALP23 (Figure 1A), such that R12 is between the Trp indole rings, while R14 is on a different face of the projection. Several factors could contribute to the variable membrane topography of GWALP23-R12. The proximity of R12 to the bilayer center is likely to impose an energetic penalty for membrane insertion, and it is furthermore plausible that the positions of the Trp indole side chains could play a significant role, for example, by obstructing water access to the R12 guanidinium group.[16] In these experiments, the identical NMR spectra observed as a function of pH indicate that the Arg guanidinium group remains charged. Indeed, because the Arg side chains undoubtedly carry a positive charge at low pH, the similar results from pH 4.5 to 7.4 indicate that the guanidinium groups remain charged in the experiments reported previously[16] and in the present work, reported here.

To better understand the control of topography of membrane-associated peptides, and to gain additional insights concerning Arg, Trp, and lipid bilayer interactions, we have tested the influence of changing the GWALP23 Trp residue locations, both with and without R14 or R12 being present. By moving each of the anchoring Trp residues, a distance corresponding to one Leu-Ala dipeptide segment toward the respective peptide terminals, an isomer of GWALP23 with an effectively longer hydrophobic helical core was constructed, acetyl-GGW^3(LA)$_8$LW^{21}GA-amide, designated GW^{3,21}ALP23 (Table 1). This peptide assumes a stable transmembrane orientation, with modest dynamics and an average tilt angle that ranges from ∼5° in DOPC to ∼20° in DLPC.[19] The rationale

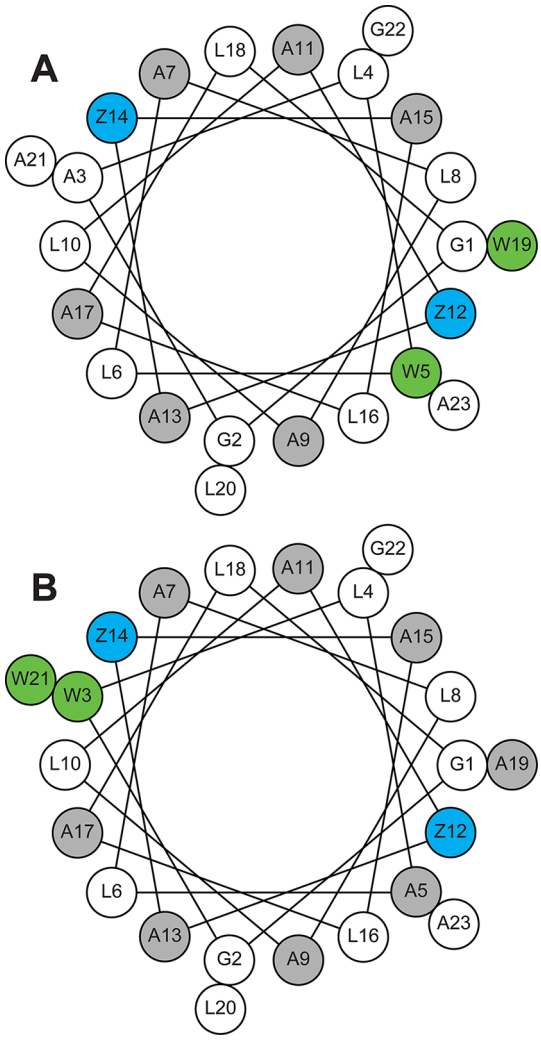

Figure 1. Helical wheel plots of GW^{X,Y}ALP23-R^Z: (A) X = 5, Y = 19; (B) X = 3, Y = 21 (Z = 12 or 14 in both (A) and (B)). Trp residues are shown in green, and ^{2}H-labeled alanines are gray. The possible locations for a single Arg are blue, with only one Arg being present in each peptide. When residues 12 and 14 are not Arg, they are Leu; see also Table 1.

for moving the Trps can be seen in an idealized helical wheel projection (Figure 1B). Switching Trp^5 to position 3 alters its radial projection by −200°, while moving Trp^{19} to position 21 alters its radial projection by +200°. As a result, the two Trp residues in GW^{3,21}ALP23 again project from one side of the helix (in fashion similar to GW^{5,19}ALP23), but now the tryptophans are located on the helix face close to R14 instead of R12 (compare Figure 1A and B). Substitutions of L12→R12 or L14→R14 in this new sequence context reverse the respective Arg positions relative to the Trp residues. Residue 12, which was between the two Trp indole rings in GW^{5,19}ALP23[16], is no longer "sandwiched" in the modified sequence. In contrast, residue 14, which was far from Trp^5 and Trp^{19}, now becomes placed radially near Trp^3 and Trp^{21}.

It is of further interest to note that the Trp−Arg separation distances are seven residues between R12 and either W5 or W19, as well as between R14 and W21. Residue R12 retains the truly central location, both in terms of the overall sequence and its position relative to the two tryptophans within each sequence. Furthermore, in the absence of the guest arginine

dx.doi.org/10.1021/jp308182b | J. Phys. Chem. B 2012, 116, 12980−12990

residues, GW[5,19]ALP23 and GW[3,21]ALP23 exhibit closely similar tilt angles in several lipid bilayer membranes, thus facilitating comparisons between the two systems.[19] Consequently, the new and expanded peptide design offers opportunities for investigating the root causes of the Arg-induced multistate behavior. Understanding the onset and loss of multistate properties for related peptide sequences in turn could provide new insights into the adaptation of transmembrane helical domains to the lipid bilayer environment.

2. MATERIALS AND METHODS

Lipids were purchased from Avanti Polar Lipids (Alabaster, AL). Peptides were synthesized on a model 433A peptide synthesizer (Applied Biosystems by Life Technologies, Foster City, CA) and cleaved from Rink resin as described previously.[16] Protected amino acids were obtained from NovaBiochem (San Diego, CA). Deuterium-enriched alanines (Ala-d_4 or Fmoc-Ala-d_3) were purchased from Cambridge Isotope Laboratories (Andover, MA). The Ala-d_4 was manually derivatized with an Fmoc group as reported earlier.[20] Typically, two ^{2}H-labeled alanines were incorporated per peptide at different isotope abundance levels. If necessary to resolve ambiguities among spectral assignments, selected peptides were prepared with only one Ala-d_4 or Ala-d_3 label. Peptides were purified on an octyl silica column (Zorbax Rx-C8, 9.4 × 250 mm, 5 μm particle size; Agilent Technologies, Santa Clara, CA) in a 92−96% methanol gradient (with 0.1% trifluoroacetic acid) over 24 min, with detection based on absorbance at 280 nm. Analytical HPLC and mass spectral data are shown in Figures S1 and S2 of the Supporting Information.

Samples (1/60, peptide/lipid ratio) for solid-state NMR spectroscopy were prepared by mechanical alignment utilizing previously reported procedures.[21] The peptide/lipid (1.3 μmol/80 μmol) mixture was deposited on glass slides (4.8 mm × 23 mm × 0.07 mm; Marienfeld; Lauda-Königshofen, Germany) from methanol:water (95:5), dried extensively, and hydrated with ^{2}H-depleted water (Cambridge) to achieve 45% hydration (w/w). Deuterium NMR spectra were obtained with a quadrupolar echo pulse sequence[22] at β = 0° and β = 90° macroscopic sample orientations using two Bruker Avance 300 spectrometers (Billerica, MA) operated at 46.1 MHz, for detection of ^{2}H resonances. The pulse time was 3.2 or 4.5 μs; echo delay 110 or 125 μs; and recycle delay 90 ms. Reduction of echo delay times below 70 μs did not reveal additional peaks in the spectra but did result in baseline distortion, most likely associated with probe ringing. Typically 700 000 transients were acquired, with the exception that 1 500 000 transients were acquired for GW[3,21]ALP23-R12 in DMPC and DOPC. Data were collected in a 32 768 point time domain, zero filled to 5120 points, and left shifted to the echo maximum. Fourier transformation was accomplished using exponential apodization with 100 Hz line broadening. Resonances were assigned on the basis of the relative peak intensities in relation to the respective isotope enrichment levels used for different alanines in the sequence. Difference spectra between double- and single-labeled peptides were sometimes employed to complete the assignments (see Figure S3 of the Supporting Information).

Deuterium NMR spectra were analyzed according to the "GALA" formalism, using the peptide rotation ρ, tilt τ, and principal order parameter S_{zz} as variables.[21,23] Angle $\varepsilon_\parallel$, defining the Ala side chain geometry in the α-helix, was fixed at 59.4° for the methyl groups[21] or 122.0° for the backbone deuterons. The value for the side chains has been previously optimized,[21] while $\varepsilon_\parallel$ for the C_αD groups was chosen as yielding the lowest RMSD of the data fit (Figure S4 of the Supporting Information). The quadrupolar coupling constant (QCC) was set to 168 kHz (backbone C_αD signals) or 56 kHz (side-chain $C_\beta D_3$ signals). In a combined analysis, due to differences in the measurement uncertainty and the kilohertz range, the backbone C_αD signals were given weights of 0.15, relative to 1.0 for the side chain $C_\beta D_3$ signals in these RMSD calculations. Dynamics were estimated using a variable S_{zz} parameter,[23] which provides a suitable treatment for GWALP23 and related membrane-associated peptides,[24] particularly when a single arginine is present.[16]

In the case of GW[3,21]ALP23-R12 in DLPC bilayers, a more explicit treatment of dynamics, based upon "Model 6" of Strandberg et al.,[23] was considered. The availability of eight Ala side-chain and five Ala backbone ^{2}H quadrupolar splittings rendered this analysis feasible, using relative weights of 0.3 for the C_αD signals and 1.0 for the side chain $C_\beta D_3$ signals. In such a calculation, rigid body motion of the peptide is modeled as Gaussian distributions of the τ and ρ angles, centered at the average values τ_0 and ρ_0 with standard deviations of σ_τ and σ_ρ, respectively. A fixed order parameter S_{zz} was set to 0.88 to approximate internal motion (the resulting product QCC × S_{zz} therefore being fixed to 49.3 kHz). A grid search was performed by varying σ_τ in the 0−30° range, σ_ρ in the 0−200° range, τ_0 from 0° to 90°, and ρ_0 from 0° to 359°. Each of the free parameters (τ_0, ρ_0, σ_τ, and σ_ρ) was incremented at 1° intervals during the grid search.

Samples for CD spectroscopy were prepared using small unilamellar vesicles (1/60, peptide/lipid) obtained by ultrasonic treatment. The peptide concentrations were in the 100 μM range and were determined by UV spectroscopy, using ε_{280} = 5600 $M^{-1}\,cm^{-1}\,Trp^{-1}$. Five scans were acquired and averaged, using a Jasco J710 spectropolarimeter (Easton, MD) operated with 1.0 mm path length, 1.0 nm bandwidth, and 20 nm/min scan rate.

Steady-state fluorescence spectra were recorded on a Perkin-Elmer LS-55 fluorescence spectrometer. Samples were prepared by 50-fold dilution of the samples that were used for CD spectroscopy. The excitation wavelength was set to 284 nm, and the emission range was 300−500 nm. Excitation and emission path lengths were 10 and 1 mm, respectively;[25] slit widths were 7.5 nm. Ten scans were acquired at 200 nm/min and averaged.

Coarse-grained molecular dynamics simulations (CG MD) of the peptides in bilayers of ∼128 DLPC or DPPC lipids were performed using the Sidekick high-throughput software,[16,26] with the MARTINI forcefield.[27] In this representation, a 4:1 mapping of non hydrogen atoms to CG particles is used, with Lennard-Jones interactions between particles based on four classes (polar, apolar, mixed polar and apolar, and charged, with subtypes describing polarity and hydrogen-bonding capabilities) and a lookup table. Lennard-Jones interactions shifted to zero at distances between 9 and 12 Å, and electrostatic interactions were shifted to zero between 0 and 12 Å. Simulations were performed with Gromacs 3.3 (www.gromacs.org). Temperature was coupled using a Berendsen thermostat at 323 K (τ_T = 1 ps), and pressure was coupled anisotropically at 1 bar (compressibility = 3 × 10^{-5} bar^{-1}, τ_P = 10 ps). The integrity of α-helices was maintained by means of dihedral restraints.[27] One hundred simulations of 200 ns duration were performed for each peptide. All-atom N terminally snorkeling forms of GW[3,21]ALP23-R12 and

GW^{5,19}ALP23-R12 were built from final snapshots in the CG-MD simulations using CG2AT.[28] Atomistic simulation of 50 ns duration was performed for each peptide in DPPC.

3. RESULTS

To investigate changes in the lipid interactions of the Arg-containing peptides caused by shifting the positions of the Trp "anchor" residues in the GW^{5,19}ALP23 framework, we have employed solid-state NMR spectroscopy using peptides specifically labeled with ^{2}H-alanine residues.[21,29] As compared to the original GW^{5,19}ALP23 sequence, GW^{3,21}ALP23 has an extended central core region, which provides two additional alanine residues for labeling and analysis (Figure 1). To verify that the peptides retain their α-helical character upon arginine incorporation, CD spectra were recorded (Figure S5 of the Supporting Information). In a manner similar to GW^{5,19}ALP23, GW^{3,21}ALP23 and also its derivatives incorporating single arginines remain substantially helical. Each Leu-to-Arg substitution leads to a small increase of the $\varepsilon_{222}/\varepsilon_{208}$ ratio from ~0.80 to ~0.84, while the overall mean residue ellipticity is either the same (R14) or somewhat diminished (R12).

To further enhance understanding of the complex balance among the peptide tilt, displacement, and arginine position, we have investigated the properties of the R12 and R14 peptides in lipids of varied hydrophobic thickness, bilayers composed of DLPC, DMPC, or DOPC lipids. Here, we employ a previously introduced approach of labeling two sequential Ala residues (separated by one leucine, or about 200° around a helical wheel projection) at different isotope abundance levels, which gives rise to two pairs of ^{2}H resonances that usually are distinguishable and often can be assigned on the basis of their relative intensities. Remarkably, both of the GW^{3,21}ALP23-Arg peptides in all three lipids exhibit strong unique pairs of ^{2}H resonances for each of the A17 and A19 side chains (Figure 2), characteristic of one conformation and one dominant average orientation of the helical peptide. Indeed, the results for GW^{3,21}ALP23-R12 contrast sharply with those for GW^{5,19}ALP23-R12, which produced multiple low-intensity signals in DOPC.[16] A similarity with other GWALP peptides is that the spectra in Figure 2 also are consistent with fast rotational averaging around the bilayer normal (peptide "precession"), as can be seen by the 2-fold reduction in the ^{2}H $\Delta\nu_q$ value for each Ala side chain when the macroscopic sample orientation is changed from $\beta = 0°$ to $\beta = 90°$ (Figure 2). Such averaging usually is observed for monomeric transmembrane peptides and is possible also for some interfacial orientations[16] and some small helix bundles.[30,31] In large aggregates, reduced rotational diffusion gives rise to powder pattern spectra.[32]

Also evident in Figure 2D is one additional pair of ^{2}H resonances for GW^{3,21}ALP23-R14 in DLPC and DMPC. These resonances, which have a large $|\Delta\nu_q|$ magnitude and likely arise from a backbone C_α deuteron, were later assigned to A17 (see below). These particular C_α–D resonances are much less intense in DOPC or when the sample orientation is $\beta = 90°$ (Figure 2); we do not yet understand the reasons for the dependence upon lipid identity and macroscopic alignment with respect to B_0. While the three-site jump motion of Ala side-chain methyl group deuterons results in a 3-fold reduction of the effective QCC, such averaging is absent for the aliphatic C_α–D groups, making possible a wider range of $\Delta\nu_q$ values. In the case of a low mobility peptide (having $S_{zz} \approx 0.9$, for example), the backbone signals therefore could span a range of ~220 kHz, as compared to only ~75 kHz for the methyl group signals. The larger $\Delta\nu_q$ span and the absence of local bond rotational averaging are also associated with increased line broadening and decreased intensity of the backbone signals (see also ref 33). To verify that the "new" resonances with large $|\Delta\nu_q|$ values indeed arise from backbone deuterons, we synthesized a single GW^{3,21}ALP23-R12 peptide with Ala-d_3 (having only C_β deuterons) present in residues A13 and A15, for comparison with an identical peptide with Ala-d_4 (having both C_β and C_α deuterons). Deuterium NMR spectra of these peptides (Figure 3) show that the signals having $|\Delta\nu_q|$ of 110 kHz are present only with Ala-d_4 and not with Ala-d_3 labeling. The signals that are absent for the case of Ala-d_3 labeling therefore indeed arise from a C_α-deuteron.

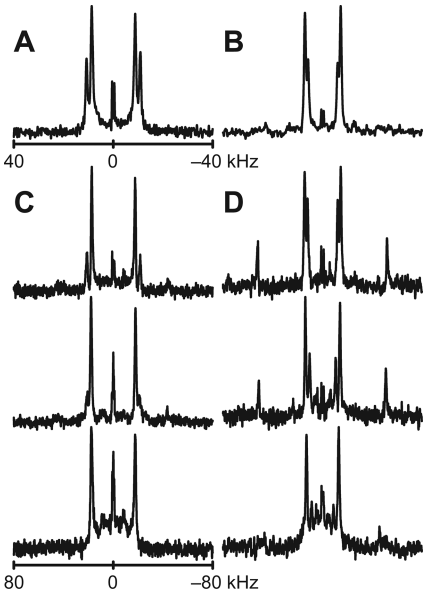

Figure 2. Deuterium NMR spectra of GW^{3,21}ALP23-R^z peptides labeled at alanines 17 (full deuteration) and 19 (partial), incorporated in (A) DLPC ($Z = 12$); (B) DLPC ($Z = 14$); (C) DLPC, DMPC, and DOPC (top to bottom; $Z = 12$); or (D) DLPC, DMPC, and DOPC (top to bottom; $Z = 14$). Sample orientation is $\beta = 90°$ (A,B) or $\beta = 0°$ (C,D). Note that the kHz scale is expanded by a factor of 2 in (A) and (B).

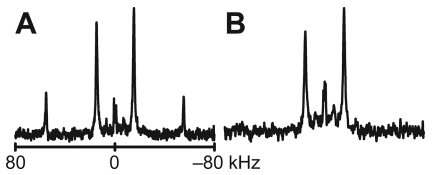

Figure 3. Deuterium NMR spectra of GW^{3,21}ALP23-R^{12} labeled at positions 13 (full deuteration) and 15 (partial deuteration) in DLPC. (A) Ala-d_4 label; (B) Ala-d_3 label. Note that two methyl signals at ~28 kHz are not resolved.

The ^{2}H quadrupolar splitting magnitudes were measured for the side-chain methyl groups of all eight core alanine residues in GW^{3,21}ALP23-R12 and GW^{3,21}ALP23-R14, each in DLPC, DMPC, and DOPC bilayer membranes. The corresponding NMR spectra are included as Supporting Information (Figures S6–S8). Many of the alanines also produced readily detectable backbone C_α deuterium signals (Figures S6–S8). The measured ^{2}H quadrupolar splitting magnitudes for Ala $C_\beta D_3$

dx.doi.org/10.1021/jp308182b | J. Phys. Chem. B 2012, 116, 12980–12990

Table 2. Alanine $C_\beta D_3$ and $C_\alpha D$ Quadrupolar Splitting (kHz) for Selected $GW^{x,y}ALP23\text{-}R^z$ Peptides Incorporated in DLPC, DMPC, or DOPC[a]

		$C_\beta D_3$ position							
peptide	lipid	5	7	9	11	13	15	17	19
$GW^{3,21}$ALP23-R12	DLPC	30.4	29.3	6.8	7.9	29.8	27.6	35.1	43.0
	DMPC	29.1	28.1	6.4	6.4	30.3	30.3	35.1	41.8
	DOPC	26.8	26.8	7.2	6.4	29.6	26.6	35.8	38.2
$GW^{3,21}$ALP23-R14	DLPC	37.7	33.1	22.2	24.7	7.6	7.6	28.9	24.2
	DMPC	26.8	28.1	13.2	20.7	12.2	0.7	27.5	21.0
	DOPC	17.9	26.6	9.9	18.4	10.6	1.2	25.4	17.1
$GW^{5,19}$ALP23-R14	DLPC		33.0	21.1	25.7	9.3	6.8	30.8	
	DMPC		30.6	14.1	21.3	10.3	3.7	29.1	
	DOPC[b]		26.6	5.5	16.0	13.1	1.3	28.0	
		$C_\alpha D$ position							
peptide	lipid	5	7	9	11	13	15	17	19
$GW^{3,21}$ALP23-R12	DLPC	106		110	169	110		89	
	DMPC			114		113			
	DOPC			117		112			
$GW^{3,21}$ALP23-R14	DLPC			103			114	103	
	DMPC			106			94	102	
	DOPC			100			84	97	
$GW^{5,19}$ALP23-R14	DLPC			107	106	115	148	106	
	DMPC			100	94	111	130	104	
	DOPC			92	82	105		96	

[a]Entries left blank were not observed in the ^2H NMR spectra. [b]Data from ref 16.

and $C_\alpha D$ groups in $GW^{3,21}$ALP23-R12 and $GW^{3,21}$ALP23-R14 in each lipid bilayer system are summarized in Table 2. Previously,[16] we reported the ^2H NMR data for labeled alanines in $GW^{5,19}$ALP23-R14 in DOPC; now in Table 2 we include also the measured $\Delta\nu_q$ values in DLPC and DMPC. Data for $GW^{5,19}$ALP23-R12 are not included because the peptide was found previously to exhibit multistate behavior in DOPC,[16] and we find similar behavior in DMPC and DLPC lipid bilayers.

An increase of the number of observed backbone ^2H signals makes it possible for the first time to incorporate this additional information for the determination of the peptide apparent orientations in the lipid bilayer membranes. The ensemble of both the C_α–D and the C_α–C_β bond vectors from the alanines is expected to provide high sensitivity concerning the tilt of a particular peptide's helix axis with respect to a given bilayer normal.

To begin a combined analysis, we sought to examine the apparent orientation of $GW^{3,21}$ALP23-R12 in DLPC, because the backbone signals in this system are observed for five alanine positions (Table 2). The joint weighted analysis of eight methyl and five backbone ^2H $|\Delta\nu_q|$ values gives an excellent fit for the side-chain methyl signals and a modest fit for the backbone signals (Figure 4). The overall fitted S_{zz} value of ~0.84 nevertheless does not quite accommodate the remarkably large $|\Delta\nu_q|$ values associated with the Ala^{11} and Ala^5 backbone signals (Figure 4B). While we note that the fit for the backbone deuterons would show moderate improvement if the value of S_{zz} were allowed to increase somewhat, we do not yet understand the basis for this observation.

Because of a decreased signal-to-noise ratio, only two backbone deuterons can be assigned unambiguously for $GW^{3,21}$ALP23-R12 in DMPC or DOPC. Because these signals for A9 and A13 are furthermore observed in the plateau region of the backbone quadrupolar wave plot, they prove not to contribute pertinent information for the GALA fits. Nevertheless, three useful backbone signals are observed for $GW^{3,21}$ALP23-R14 and four or five for $GW^{5,19}$ALP23-R14 in

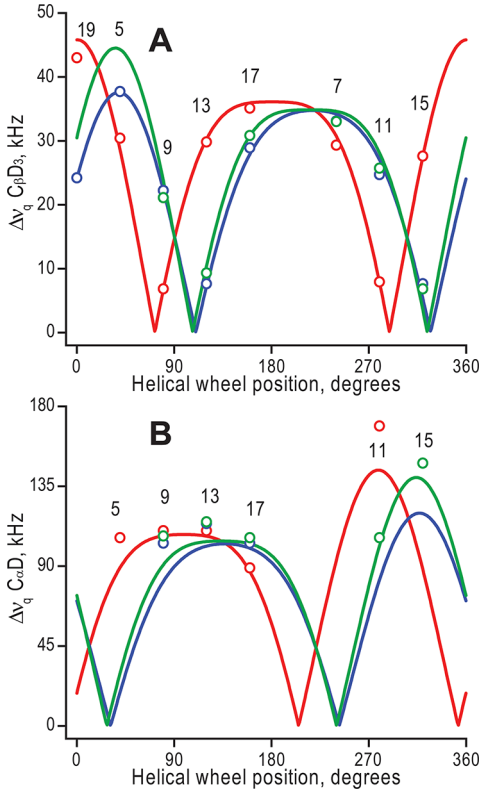

Figure 4. GALA quadrupolar wave plots for Ala methyl and backbone groups of $GW^{3,21}ALP23\text{-}R^z$ and $GW^{5,19}$ALP23-R14 in DLPC. (A) Methyl signals for $Z = 12$ (red), $Z = 14$ (blue), and $GW^{5,19}$ALP23-R14 (green). (B) Backbone signals for $Z = 12$ (red), $Z = 14$ (blue), and $GW^{5,19}$ALP23-R14 (green). Alanine positions are indicated.

dx.doi.org/10.1021/jp308182b | J. Phys. Chem. B 2012, 116, 12980–12990

all three lipids, making it possible to employ these data within the analysis. The best fits for the weighted analysis are summarized in Table 3 and Figures 4 and 5. The observed backbone signals furthermore provide valuable data points for more extensive treatments of the peptide dynamics (see Discussion).

Table 3. GALA Fit Results[a]

	GALA fit results				
				RMSD, kHz	
(lipid) peptide	S_{zz}	τ, deg	ρ, deg	$C_\beta D_3$	$C_\alpha D$
(DLPC)					
$GW^{3,21}$ALP23-R12	0.86	29.8	224	1.3	13.6
$GW^{3,21}$ALP23-R14	0.85	25.2	262	1.3	13.0
$GW^{5,19}$ALP23-R14	0.83	30.0	259	2.1	10.0
(DMPC)					
$GW^{3,21}$ALP23-R12	0.94	26.5	223	2.3	0.1
$GW^{3,21}$ALP23-R14	0.88	19.5	253	1.2	17.7
$GW^{5,19}$ALP23-R14	0.81	25.8	252	1.6	12.4
(DOPC)					
$GW^{3,21}$ALP23-R12	0.96	24.1	223	1.9	3.3
$GW^{3,21}$ALP23-R14	0.94	15.2	253	1.5	20.2
$GW^{5,19}$ALP23-R14	0.94	16.1	246	1.3	13.3

[a]Alanine $C_\beta D_3$ and $C_\alpha D$ ^2H quadrupolar splittings were differently weighed for the RMSD calculations to obtain the apparent tilt and rotation angles as well as S_{zz}. Angles $\varepsilon_\parallel$ and $\varepsilon_\perp$[21] were fixed at 59.4° and −43°, respectively, for $C_\beta D_3$; the corresponding values for $C_\alpha D$ were 122.0° and 55°.

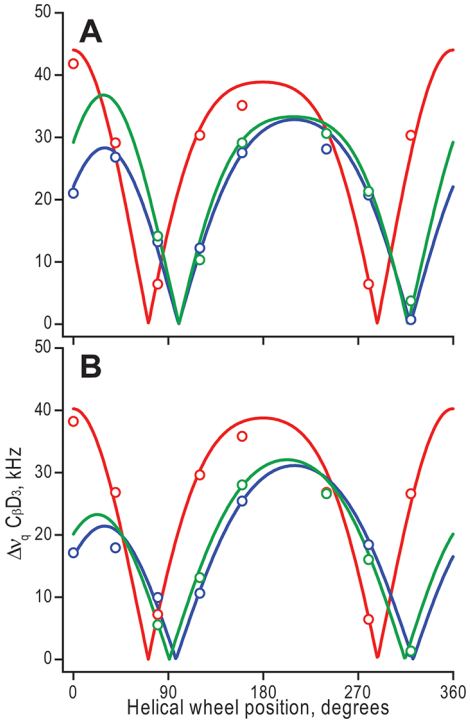

Figure 5. GALA quadrupolar wave plots for Ala methyl groups of $GW^{3,21}$ALP23-R^z and $GW^{5,19}$ALP23-R14 in (A) DMPC, and (B) DOPC. The colors represent Z = 12 (red), Z = 14 (blue), and $GW^{5,19}$ALP23-R14 (green).

From the range of magnitudes observed among the quadrupolar splittings, it is apparent that the Arg-containing peptides are significantly tilted with respect to the lipid bilayer normal. Indeed, the GALA analysis of quadrupolar splittings returns tilt angles as large as 30° (Table 3). Low RMSD values for fitting the side-chain quadrupolar splittings suggest that the α-helical conformation is maintained throughout the core sequence, between the Trp residues.[34] (The higher RMSD values for backbone groups may reflect limitations in the treatment of the dynamics; see Discussion.) Visual comparisons of the best-fit quadrupolar waves for $GW^{3,21}$ALP23-R14 and $GW^{3,21}$ALP23-R12 reveal that the tilt magnitudes are similar yet the ρ values are noticeably different, as the R12 and R14 curves are about 30−40° out of phase. Conversely, the best-fit curves for both -R14 peptides nearly overlap, indicating highly similar orientations for the $W^{5,19}$ and $W^{3,21}$ peptides when R14 is present. The peptide rotation (direction of tilt) is in these cases determined by the sequence position of the lone Arg residue. (Because of the rather shallow RMSD minimum as a function of S_{zz}, the apparent τ and ρ angles for $GW^{5,19}$ALP23-R14 in DOPC differ marginally from a previous report.[16])

Several general trends emerge from the GALA curves for the Arg-containing peptides. As the lipid bilayer thickness increases, there is a rise in the best-fit value of S_{zz}, suggesting less extensive or lower amplitude motions for the peptides in DOPC bilayers. Moreover, for the -R14 peptides in DOPC, the RMSD function does not reach a minimum over the whole range of S_{zz}, but rather would fit best at S_{zz} values close to unity. The rotation angle furthermore does not change significantly with lipid identity for either the -R14 or the -R12 series, and both -R14 peptides exhibit similar apparent tilt angles in corresponding lipids.

As the hydrophobic thickness of the membrane increases, there is a marked decrease in the spectral quality for $GW^{3,21}$ALP23-R12, where the Arg residue is central within the sequence. Nevertheless, the trends for the peak assignments in the spectra for $GW^{3,21}$ALP23-R12 in DMPC and DOPC match those in DLPC, for both β = 0° and β = 90° sample orientations. On the other hand, $GW^{3,21}$ALP23-R14 retains a good signal-to-noise ratio in each lipid (Table 2; Figures S6−S8). GALA analysis reveals that in DMPC and DOPC a transmembrane topography is retained for both $GW^{3,21}$ALP23-R14 and $GW^{3,21}$ALP23-R12 (Figure 5). The tilted transmembrane orientations furthermore are fitted with excellent RMSD values that are below 1.5 kHz for the side-chain methyl groups, attesting to highly helical structures (Table 3).

The differences in preferred average transmembrane orientation among the single-Arg $GW^{5,19}$ALP23-R14 and $GW^{3,21}$ALP23-R14 and -R12 peptides are apparent in RMSD contour plots, graphed as a function of the apparent τ and ρ angles for each peptide in DLPC, DMPC, and DOPC lipid bilayer membranes (Figure 6). $GW^{3,21}$ALP23-R12, with the most centrally located Arg, exhibits a more narrow range of tilt angles in the three lipids, as the contour levels cluster in a narrow range (Figure 6A). Conversely, $GW^{3,21}$ALP23-R14 and $GW^{5,19}$ALP23-R14 are more sensitive to the membrane hydrophobic thickness, with the R14 peptides adopting apparent tilt angles that span a range of 10° or more (as opposed to ∼5° for $GW^{3,21}$ALP23-R12). These trends are replicated in the CG MD simulations (see below). When the host lipid is changed, the peptide rotation or direction of tilt (ρ angle) does not change much for any of the peptides, as the preferred orientation of the helix is most likely dictated by the radial position of the single Arg residue. Indeed, the ρ angle for the two different R14 peptides is essentially identical in each lipid bilayer that was tested. The ρ value for $GW^{3,21}$ALP23-R12

dx.doi.org/10.1021/jp308182b | J. Phys. Chem. B 2012, 116, 12980−12990

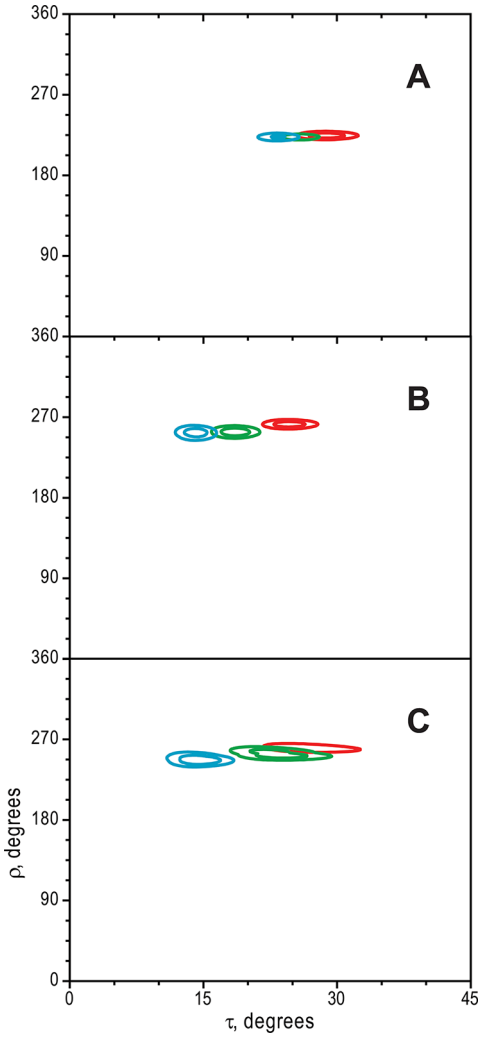

Figure 6. RMSD contour plots for GW^{x,y}ALP23-R^{z} in DLPC (red), DMPC (green), and DOPC (blue). (A) $X = 3$, $Y = 21$, $Z = 12$; (B) $X = 3$, $Y = 21$, $Z = 14$; (C) $X = 5$, $Y = 19$, $Z = 14$. Contours are plotted at 1, 2, and 3 kHz.

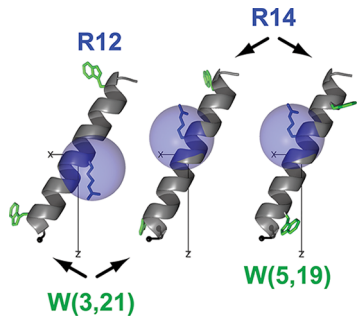

Figure 7. Molecular models of tilted GW^{x,y}ALP23-R^{z} in DLPC. Black spheres indicate the C_α atom of G^1. The radii of shaded blue spheres (centered at C_β of arginine) correspond to a range of possible extended conformations for each Arg side chain.

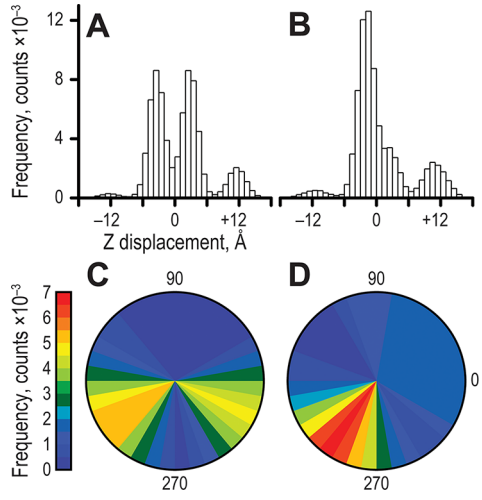

Figure 8. CG MD simulations. (A) Displacement of GW^{3,21}ALP23-R12 relative to DLPC bilayer center. (B) Same as (A), but for GW^{3,21}ALP23-R14. (C) Distribution of rotation angles of GW^{3,21}ALP23-R12 in DLPC. (D) Same as (C), but for GW^{3,21}ALP23-R14.

also does not change with the lipid thickness (or unsaturation, in DOPC). Visualization of the tilted peptides yields models where Arg^{12} could snorkel (only) toward the N-terminal leaflet. By contrast, it appears that only C-terminal snorkeling is accessible for the Arg^{14} side chain, regardless of whether positions (5, 19) or (3, 21) are chosen for the locations of the Trp anchor residues (Figure 7).

The NMR methods are sensitive to peptide orientation but not to translocation. To probe this possibility for GW^{3,21}ALP23-Arg peptides, we performed CG MD simulations in DLPC and DPPC bilayer membranes. Both the -R12 and the -R14 substituted GW^{3,21}ALP23 peptides adopted transmembrane orientations 80−85% of the time in calculations that spanned 100 × 200 ns. The trends for GW^{3,21}ALP23-R14 are similar to those observed previously with GW^{5,19}ALP23-R14.[16] Indeed, both R14 peptides undergo vertical displacement toward the C-terminal leaflet (Figure 8) by 2−4 Å, which may be understood if the side-chain snorkeling is directional yet not sufficient by itself for the positively charged Arg guanidinium group to reach an aqueous interface, causing also the peptide to move its center of mass. The rotation angle for GW^{3,21}ALP23-R14 is well-defined with a sharp maximum (Figure 8D), and indeed is very close to that of GW^{5,19}ALP23-R14 obtained by CG MD,[16] in agreement with the NMR experiments for both R14 peptides (Figures 4−6). The CG-MD simulations show a single orientation of GW^{3,21}ALP23-R14 in the membrane, with tilts of ∼36° in DLPC and ∼25° in DPPC. The trend agrees with the experimentally observed sensitivity of the peptide tilt to membrane thickness.

On the other hand, CG-MD simulations show a bimodal distribution for GW^{3,21}ALP23-R12 in DLPC (Figure 8), apparently displaying both C- and N-terminal peptide center-of-mass shifts and Arg snorkeling orientations. The peptide behavior in the CG MD simulations resembles that of GW^{5,19}ALP23-R12 in DOPC or DPPC, although the distributions are now notably narrower and better defined when the tryptophans are farther removed from R12. While CG MD reports two orientations of GW^{3,21}ALP23-R12, it can be seen from the intensities of the rotation plot (Figure 8C) that one of the rotation angles is more prevalent. This particular population, corresponding to R12 snorkeling toward the N-terminal, is the one observed by ^{2}H NMR (see Discussion). While the minor population from CG-MD is a puzzle, one notes that the distributional narrowing and the predominant population from the CG MD simulations agree with experiment. A known limitation of the CG model employed here is

dx.doi.org/10.1021/jp308182b | J. Phys. Chem. B 2012, 116, 12980−12990

that it does not reproduce the preference of arginine residues to snorkel N terminally.[16] The CG limitation could be the cause of the minor population. On the basis of the limitation, we would expect that the preference for N-terminal snorkeling is underestimated and should be even stronger than suggested in Figure 8C, a result that would be consistent with the NMR data. The tilt of $GW^{3,21}$ALP23-R12 is measured from the simulations to be ∼35° in DLPC and ∼28° in DPPC. The ∼20% change in the helix tilt compares well with the results from the NMR experiments (Table 3). Notably, both the R12 and the R14 $W^{3,21}$ peptides induce bilayer deformations in the vicinity of the Arg residue (which snorkels ∼3 Å in each case), as a result of polar contacts between the phospholipid headgroup and the Arg guanidinium group. This deformation is sufficient to allow for water access to the charged side chain, as observed previously[16] with $GW^{5,19}$ALP23-R12 and -R14.

To confirm the observations from CG-MD simulations, all-atom N terminally snorkeling forms of both $GW^{3,21}$ALP23-R12 and $GW^{5,19}$ALP23-R12 were built from final snapshots in the CG-MD simulations using CG2AT,[28] and 50 ns of atomistic simulation was performed for each peptide in DPPC. When starting from a transmembrane configuration, $GW^{5,19}$ALP23-R12 remained stable in the membrane over the course of the 50 ns simulation, but the W5 side chain was competing with the R12 side chain for access to the phosphate headgroups in the interfacial region. Access of R12 in $GW^{5,19}$ALP23-R12 to the aqueous interface was therefore incomplete over the course of the simulation (Figure S9). In contrast, R12 in $GW^{3,21}$ALP23-R12 maintained good access to the aqueous interface over the 50 ns, aided by deformation of the bilayer, which was induced by interactions between the phosphate head groups and the arginine side chain (Figure S9). The access of R12 may also be assisted, in part, by partial unfolding of the termini of $GW^{3,21}$ALP23-R12, observed during the 50 ns, during which W3 and W21 furthermore remain on the opposite helix face from the location of the R12 snorkeling. (Final snapshots from these calculations are shown in Figure S9 of the Supporting Information).

To probe experimentally the peptide asymmetric position in lipid bilayer membranes, we have measured intrinsic Trp fluorescence (Figure 9), a notably sensitive indicator of the environment polarity.[35] The interpretation of fluorescence data is complicated by the presence of two tryptophans in GWALP23 peptides. Qualitative comparisons indicate that the emission maximum (344 nm) is similar for $GW^{3,21}$ALP23 itself and the -R12 analogue in DLPC, but some 3 nm higher for the -R14 analogue, suggesting that the latter peptide adjusts its transverse position for R14 to reach toward an aqueous phase, similar to CG MD observations (Figure 9B). The bimodal distribution, observed by CG MD for $GW^{3,21}$ALP23-R12, would suggest little net peptide displacement, on average, in agreement with the fluorescence results. In thicker DOPC membranes, $GW^{3,21}$ALP23 yields λ_{max} of 340 nm, while both the -R12 and the -R14 derivatives exhibit much higher values (347 and 349 nm, respectively), which approach λ_{max} of Trp in water (Figure 9A).

The full width at half-maximum (fwhm) for the fluorescence emission provides additional insight into the peptide behavior, as peptide "lifting" with respect to the lipid bilayer center would essentially move one Trp deeper into the bilayer, while transferring the other one to more polar media. The net result would be an expected broadening of the spectra. Indeed, the fwhm values (Figure 9C) suggest heterogeneous environments

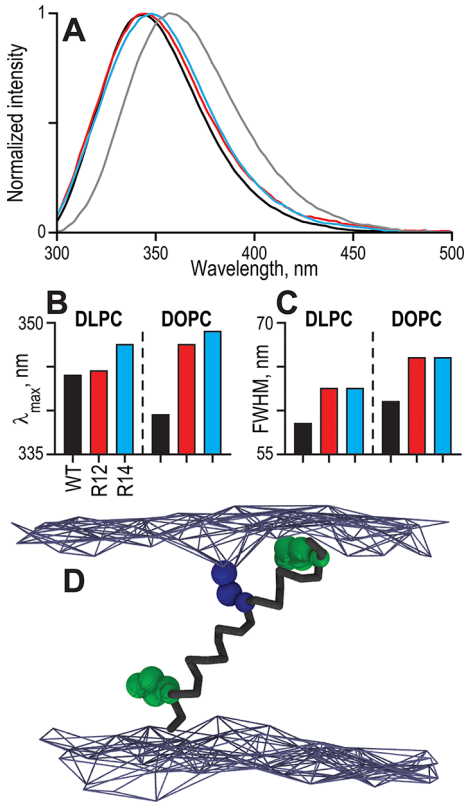

Figure 9. Steady-state fluorescence. (A) Fluorescence spectra of $GW^{3,21}$ALP23-R^z in DLPC; (B) emission maxima; and (C) full width at half-maximum values. Gray line in (A) is tryptophan in water. Other colors are consistent through panels A–C. WT refers to the host $GW^{3,21}$ALP23 peptide without arginine substitutions. Panel D illustrates a CG MD simulation result for $GW^{3,21}$ALP23-R14 in DLPC, suggesting not only that W3 is more buried than W21, but also that membrane deformation allows water access to R14 in the tilted peptide.

for the Trp residues in $GW^{3,21}$ALP23-$R^{(12\ or\ 14)}$ peptides, in comparison with the native sequence when no Arg is present. Such behavior is particularly manifest in DOPC, where the fwhm for both Arg-containing peptides is ∼5 nm larger than for the parent $GW^{3,21}$ALP23. For comparison, a CG MD simulation of $GW^{3,21}$ALP23-R14 in DLPC shows an asymmetric distribution of the Trp residues, suggesting "lifting" of the peptide, along with bilayer deformation to accommodate the access of water and phosphate head groups to the R14 residue in the tilted peptide (Figure 9D).

4. DISCUSSION

The consequences of incorporating a single arginine into $GW^{5,19}$ALP23 differ dramatically depending on whether L12 or L14 is changed to Arg[16]. The R14 variant remains transmembrane with a larger tilt angle in a different direction from the peptide without Arg, while the R12 analogue populates multiple states with respect to a DOPC bilayer membrane. Here, we have examined structurally isomeric $GW^{3,21}$ALP23-R12 and -R14 peptides, with the aim of elucidating the reasons for such behavior. Remarkably, both of the new sequences adopt well-defined transmembrane orientations, contrasting sharply with multiple populations that were observed for $GW^{5,19}$ALP23-R12. The transmembrane topography of $GW^{3,21}$ALP23-R12 indicates that a single arginine residue

dx.doi.org/10.1021/jp308182b | J. Phys. Chem. B 2012, 116, 12980–12990

indeed can be tolerated in the central position of a transmembrane α-helix, under certain conditions, although not within GW^{5,19}ALP23-R12. A notable structural feature of GW^{5,19}ALP23-R12 is the spatial arrangement of the Trp and Arg side chains. With the large W5, R12, and W19 side chains all projecting from the same face of the α-helix, the R12 guanidinium group appears to be effectively sandwiched between the two bulky aromatic groups of tryptophan. Adjustment of this motif by shifting the Trp residues from W^{5,19} to the opposite helix face (W^{3,21}) proves to be sufficient to stabilize the transmembrane helix orientation even when R12 is present. To the extent that moving the tryptophans seems to "rescue" R12 from a tryptophan "cage", it is of interest to ask what happens to R14 in GW^{3,21}ALP23-R14? Once again, the Trp and Arg side chains project from the same side of a helix, but now the tryptophans are farther apart. It is conceivable that the increased spacing between the Trp residues effectively enlarges the cage and may thereby enhance the access of R14 to a polar environment (as compared to the limited access of R12 in GW^{5,19}ALP23-R12). Whatever the detailed molecular cause, the GW^{3,21}ALP23-R14 peptide helix is observed to adopt a major transmembrane orientation. With respect to the putative "cage" formed by W5 and W19, we do not expect direct Arg−Trp interactions, because the distances from indole to R12 are too large (two helical turns). Rather, we think that the major effect of the aromatic Trp rings is to interfere with water access to the guanidinium group of Arg; in this sense, W5 and W19 are more restrictive than W3 and W21.

Both adjustments, opening or enlarging the "cage", seem to work fine in lipid bilayers of different thickness, a noteworthy feature here because the decrease of lipid acyl chain length alone did not ensure formation of a dominant state for GW^{5,19}ALP23-R12. Indeed, the analysis of the GW^{3,21}ALP23-R^z helix orientations suggests that in each case the R12 or R14 guanidinium group can reach the aqueous phase by adjusting the magnitude and direction of the helix tilt. Because of an Arg residue being close to the peptide center, Arg side-chain snorkeling to the surface requires large tilt angles, which indeed were deduced (Figure 6, Table 3) from the solid-state NMR spectra and the CG MD simulations. The tilt angles are largest for GW^{3,21}ALP23-R12, presumably due to the truly central location of the arginine. Notably, this peptide exhibits a more shallow dependence of the tilt magnitude upon lipid bilayer thickness (Table 3), suggesting that alternative mechanisms of adaptation also take place. It is important to note that, although the major driving force defining the tilt of GW^{x,y}ALP23-R^z peptides arises from the Arg residue, the anchoring Trp residues also contribute. Tryptophans have preferences for the membrane−water interface, and their displacement away from this region will impose a penalty on the system. It is possible that the maximum observed tilt value of 30°−35° may approach an upper limit for a 23-residue peptide with single Trp anchors near each end, and that further adaptation is therefore achieved by side-chain reorientations and by translating the peptide along the bilayer normal.[15,16]

The situation is somewhat different when the arginine is moved two positions toward the C-terminal to give the GW^{5,19}ALP23-R14 and GW^{3,21}ALP23-R14 peptides, which exhibit a steeper dependence of the tilt angle on lipid bilayer thickness, with τ values that range from 15° to 25°. R14 is located closer to the peptide C-terminus; however, due to the helix geometry in which the C_α−C_β bond vectors project toward the N-terminus, the R14 side chain needs to reorient to enable its snorkeling toward the C-terminus. It follows from the identical rotation angles of the R14 peptides that the responses are similar, irrespective of which helix face is occupied by the Trp residues. The strikingly identical rotation angles also imply that oscillating motions about the helix axis are restricted and therefore do not substantially average the NMR observables for these particular peptides.

It is intriguing that the Arg-containing analogues of GW^{x,y}ALP23 display prominent backbone C_αD signals at selected alanine positions. Although Ala-d_4 labels have been used routinely for many experiments, backbone C_α−D resonances nevertheless have generally not been observed for WALP-like peptides, except when Pro or Arg is present in the sequence.[16,34] Here, we have sought to employ the orientational constraints from these additional signals in concert with the Ala $C_\beta D_3$ constraints to help deduce the orientations of the respective peptides. In this context, several puzzles remain with respect to the backbone C_α−D resonances. Why have such resonances often not been observed in the ^{2}H NMR spectra of many WALP-like and GWALP-like peptides? Why are selected C_α−D resonances for GW^{x,y}ALP23-R^z peptides observed only when β = 0° and not when β = 90° (Figure 2)? The dependence on sample orientation suggests a dynamic explanation. Why does a major enhancement of the C_α−D signal intensity at β = 0°, accompanied by line narrowing, occur over a fairly small frequency range of $\Delta\nu_q$ between 95 and 115 kHz, corresponding to angle θ of 38.5° ± 1.5°. Outside of this range, the backbone signals are either not detectable or observed only as broad, low-intensity peaks for samples oriented with β = 90° and not β = 0°. The dynamic features that underlie these observations merit further investigation. Why do some of the C_α−D resonances for GW^{x,y}ALP23-R^z peptides appear so sharp (narrow), when the equivalent resonances for gramicidin channels in oriented bilayers are notably weak and broad?[33,36] Why does it seem that the backbone C_αD quadrupolar splittings "could" be better fit by assuming a somewhat higher S_{zz} value, instead of an expected lower S_{zz} value for the C_α−D bond? Indeed, dipolar coupling measurements have revealed that C−H and N−H bonds in ubiquitin fit the NMR data with either slightly "longer" effective bond lengths, or equivalently about 6% smaller S values, as compared to C−C or C−N bonds.[37] It is therefore not surprising that C_β−D_3 and C_α−D bonds in GWALP peptides should contribute different local components to the overall S_{zz}, but the trend for the backbone based on the GALA analyses of peptide orientation seems to be in the wrong direction (Figure 4). We do not understand the basis for this observation. Additionally, the value of QCC may differ for different C−D bonds.[38,39] In addition to bond librations, another important factor will be the angle of interaction between B_o and a particular bond, noted above. Together the observations point toward complex yet incompletely understood distinctions among the C_β−D_3 and C_α−D bonds with respect to local dynamics, whole-molecule motion, methyl-group rotation, molecular orientation, and sample orientation with respect to B_o. The dynamic features that underlie these observations merit further investigation.

Despite the above caveats, the backbone signals provide valuable additional data points for confirming the peptide orientation. Moreover, even when the side-chain methyl-group quadrupolar splittings are allowed to dominate, in a weighted analysis, the resulting backbone RMSD values remain on the

order of 10% or less (Table 3), indicating substantial agreement.

To provide estimates of individual components of the whole peptide motion, we have completed an explicit dynamics analysis of GW[3,21]ALP23-R12 in DLPC. The calculations were performed in two ways: first, using only the side-chain $C_\beta D_3$ $\Delta\nu_q$ values, and second, using a weighted combination of eight side-chain and five backbone $C_\alpha D$ backbone signals, using the same S_{zz} = 0.88 for both. In the latter case, RMSD was calculated according to:

$$\mathrm{RMSD} = \sqrt{\frac{\sum_{N_{CD_3}} (\Delta\Delta\nu_q)^2 + \sum_{N_{CD}} (0.3\cdot\Delta\Delta\nu_q)^2}{N_{CD_3} + N_{CD}}}$$

In the above equation, $\Delta\Delta\nu_q$ is the difference between the observed and calculated values, and N is the number of data points.

The results of the explicit dynamics analysis (Figure 10) show widespread agreement with the GALA analysis. The overall orientation and dynamics are not sensitive to whether or not the backbone signals are included in the calculations, or to the relative weighing factors. Small oscillations about the average τ_0 and ρ_0 values (σ_τ of 4−7° and σ_ρ of 6−11°) give the best fits (Figure 10), consistent with an order parameter not much below 0.88. This is important, when considering that explicit dynamics does not lead to lower RMSD or change the deduced values of τ_0 and ρ_0 when the $C_\alpha D$ data are included. Furthermore, the semistatic GALA analysis of either backbone or side-chain signals is sufficient to determine the τ_0 and ρ_0 values for the peptides considered here.

The CG MD simulations offer an opportunity for detailed views of the systems under examination. Importantly, the simulations closely reproduce the primary peptide orientations deduced from solid-state NMR. Furthermore, CG MD offers valuable insights into significant other aspects, such as membrane deformation, peptide lifting from the center of the lipid bilayer, and water defects. For both Arg-containing peptides, a bilayer thinning of ∼3 Å was observed in simulations (relative to bilayers with unmodified GW[3,21]ALP23), leading to more peptide−phosphate and peptide−water contacts. In the case of GW[3,21]ALP23-R12, CG MD predicts a multistate response of the system, a minor population with C-terminal snorkeling of R12, and a different ρ_0 angle (Figure 8C), which was not detected by solid-state NMR, in addition to the major population with N-terminal snorkeling of R12 and the same ρ_0 angle as detected by solid-state NMR. While the situation will require further investigation, we note once again the limitation of the CG model in which C-terminal snorkeling is overestimated.[16] Despite the limitation, the CG model nevertheless predicts a favoring of N-terminal snorkeling for the Arg in GW[3,21]ALP23-R12, and the agreement with the NMR data is moreover likely to be stronger than is suggested in Figure 8C.

While the solid-state NMR experiments do not provide direct information on peptide transverse shifts in the membrane, such data can be obtained by alternative techniques. Nevertheless, the design of GWALP23 peptides means that the overall fluorescence spectra result from superposition of contributions from the individual tryptophans. For this reason, the spectral comparisons among the different peptides may be more informative than any one individual spectrum. In this context, the Arg-containing peptides exhibit a red shift in the

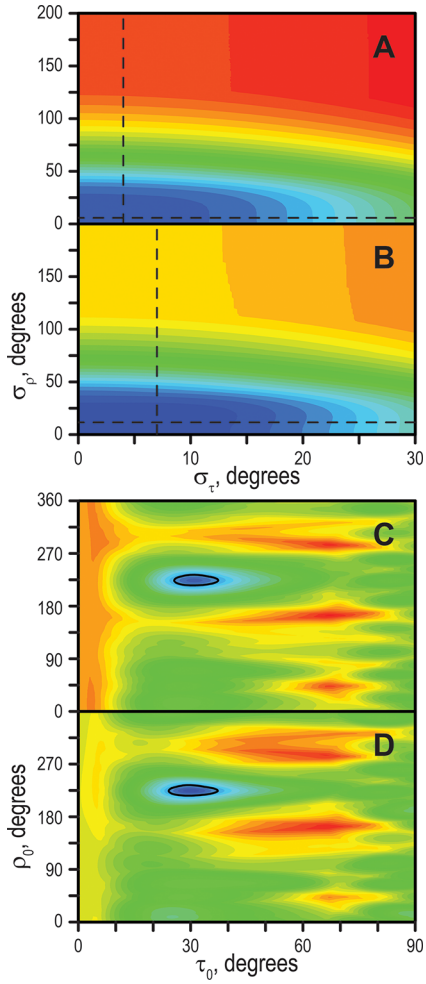

Figure 10. Explicit dynamics analysis of GW[3,21]ALP23-R12 in DLPC, showing the standard deviations of Gaussian distributions (A,B) and their centers (C,D). Analyzed data included either both $C_\beta D_3$ and $C_\alpha D$ signals (A,C) or $C_\beta D_3$ signals alone (B,D). Dashed lines in (A) and (B) indicate the best fit σ_τ and σ_ρ, which were used for generating the plots in (C) and (D), respectively. Color scale is identical between (A) and (B) (0−28 kHz) and between (C) and (D) (0−31 kHz). Color increments are at 1 kHz; solid line in (C), (D) is drawn at 5 kHz level. Best fits (τ_0, σ_τ, ρ_0, σ_ρ) are (31, 4, 224, 6) for the combined $C_\beta D_3$ + $C_\alpha D$ set and (30, 7, 224, 11) for the $C_\beta D_3$ set alone.

Trp emission λ_{max}, indicating a more polar environment for at least one of the two Trp residues. The increase in the spectral width further indicates heterogeneous environments of the two tryptophans, as expected for a peptide positioned asymmetrically in the membrane. In addition to the red shift, the more polar exposed Trp may also have a higher quantum yield, which could then cause a shifting of the "average" λ_{max}, in addition to broadening the spectra.

The single, central, Arg residue introduced within GWALP23-R12, acetylGGALW[5]LALALAR[12]ALALALW[19]-LAGA-amide, brings about multistate behavior and induces the peptide to exit from a bilayer membrane of DOPC.[16] In this Article, we report that the isolated Arg can be "rescued", with restoration of a stable, tilted transmembrane orientation for the peptide when the Trp anchors are moved from residues (5, 19) to residues (3, 21). The results reinforce the concept of multiple mechanisms by which Arg can "escape" or exit from the bilayer center. Coarse-grained molecular dynamics simulations and solid-state NMR experiments show substantial

dx.doi.org/10.1021/jp308182b | J. Phys. Chem. B 2012, 116, 12980−12990

agreement on these principles, although a difference remains to be resolved (with future work) concerning whether a second minor peptide rotation and Arg snorkeling state is accessible for GW[3,21]ALP23-R12. The corresponding R14 analogues, regardless of having Trp anchors located at positions (5, 19) or (3, 21), display single-state transmembrane behavior in DLPC, DMPC, and DOPC; as deduced and agreed by both NMR experiment and CG MD simulation, with a tilt magnitude that scales with the bilayer thickness. The relative positions of the Trp and Arg residues together are crucial for the detailed protein/lipid interactions, as reflected by the properties of these transmembrane helices.

■ ASSOCIATED CONTENT

Supporting Information

Physical data for GW[3,21]ALP23-Arg peptides (HPLC, mass spectra). Deuterium NMR spectra of peptides in DLPC, DMPC, and DOPC. Circular dichroism spectra. Snapshots from all-atom simulations for selected peptides. This material is available free of charge via the Internet at http://pubs.acs.org.

■ AUTHOR INFORMATION

Corresponding Author

*Tel.: (479) 575-4976. Fax: (479) 575-4049. E-mail: rk2@uark.edu.

Notes

The authors declare no competing financial interest.

■ ACKNOWLEDGMENTS

This work was supported in part by grants from the U.S. National Science Foundation (MCB-0841227), the Oxford Center for Integrative Systems Biology, the BBSRC and MRC, the Oxford Supercomputing Center, and the Arkansas Biosciences Institute. The peptide and NMR facilities were supported by NIH grants GM103429 and GM103450.

■ ABBREVIATIONS

CD, circular dichroism; CG MD, coarse-grained molecular dynamics; DLPC, 1,2-dilauroyl-*sn*-glycero-3-phosphocholine; DMPC, 1,2-dimyristoyl-*sn*-glycero-3-phosphocholine; DOPC, 1,2-dioleoyl-*sn*-glycero-3-phosphocholine; fwhm, full width at half-maximum; Fmoc, fluorenylmethoxycarbonyl; GALA, geometric analysis of labeled alanines; PISEMA, polarization inversion with spin exchange at magic angle; QCC, quadrupolar coupling constant; P/L, peptide to lipid ratio; RMSD, root mean squared deviation

■ REFERENCES

(1) Bartlett, G. J.; Porter, C. T.; Borkakoti, N.; Thornton, J. M. *J. Mol. Biol.* **2002**, *324*, 105−121.
(2) Doyle, D. A.; Morais Cabral, J.; Pfuetzner, R. A.; Kuo, A.; Gulbis, J. M.; Cohen, S. L.; Chait, B. T.; MacKinnon, R. *Science* **1998**, *280*, 69−77.
(3) Sine, S. M.; Wang, H. L.; Bren, N. *J. Biol. Chem.* **2002**, *277*, 29210−29223.
(4) Loladze, V. V.; Ermolenko, D. N.; Makhatadze, G. I. *Protein Sci.* **2001**, *10*, 1343−1352.
(5) Takayama, Y.; Castaneda, C. A.; Chimenti, M.; Garcia-Moreno, B.; Iwahara, J. *J. Am. Chem. Soc.* **2008**, *130*, 6714−6715.
(6) Karp, D. A.; Stahley, M. R.; Garcia-Moreno, B. *Biochemistry* **2010**, *49*, 4138−4146.
(7) Swartz, K. J. *Nature* **2008**, *456*, 891−897.
(8) Hessa, T.; Meindl-Beinker, N. M.; Bernsel, A.; Kim, H.; Sato, Y.; Lerch-Bader, M.; Nilsson, I.; White, S. H.; von Heijne, G. *Nature* **2007**, *450*, 1026−1030.
(9) Dorairaj, S.; Allen, T. W. *Proc. Natl. Acad. Sci. U.S.A.* **2007**, *104*, 4943−4948.
(10) MacCallum, J. L.; Bennett, W. F.; Tieleman, D. P. *Biophys. J.* **2008**, *94*, 3393−3404.
(11) Bechinger, B. *J. Mol. Biol.* **1996**, *263*, 768−775.
(12) Aisenbrey, C.; Kinder, R.; Goormaghtigh, E.; Ruysschaert, J. M.; Bechinger, B. *J. Biol. Chem.* **2006**, *281*, 7708−7716.
(13) Hunt, J. F.; Rath, P.; Rothschild, K. J.; Engelman, D. M. *Biochemistry* **1997**, *36*, 15177−15192.
(14) Andreev, O. A.; Dupuy, A. D.; Segala, M.; Sandugu, S.; Serra, D. A.; Chichester, C. O.; Engelman, D. M.; Reshetnyak, Y. K. *Proc. Natl. Acad. Sci. U.S.A.* **2007**, *104*, 7893−7898.
(15) Krishnakumar, S. S.; London, E. *J. Mol. Biol.* **2007**, *374*, 1251−1269.
(16) Vostrikov, V. V.; Hall, B. A.; Greathouse, D. V.; Koeppe, R. E., II; Sansom, M. S. P. *J. Am. Chem. Soc.* **2010**, *132*, 5803−5811.
(17) Killian, J. A.; Salemink, I.; de Planque, M. R.; Lindblom, G.; Koeppe, R. E., II; Greathouse, D. V. *Biochemistry* **1996**, *35*, 1037−1045.
(18) Vostrikov, V. V.; Grant, C. V.; Daily, A. E.; Opella, S. J.; Koeppe, R. E., II. *J. Am. Chem. Soc.* **2008**, *130*, 12584−12585.
(19) Vostrikov, V. V.; Koeppe, R. E., II. *Biochemistry* **2011**, *50*, 7522−7535.
(20) ten Kortenaar, P. B. W.; Van Dijk, B. G.; Peeters, J. M.; Raaben, B. J.; Adams, P. J. H. M.; Tesser, G. I. *Int. J. Pept. Protein Res.* **1986**, *27*, 398−400.
(21) van der Wel, P. C.; Strandberg, E.; Killian, J. A.; Koeppe, R. E., II. *Biophys. J.* **2002**, *83*, 1479−1488.
(22) Davis, J. H.; Jeffrey, K. R.; Bloom, M.; Valic, M. I.; Higgs, T. P. *Chem. Phys. Lett.* **1976**, *42*, 390−394.
(23) Strandberg, E.; Esteban-Martin, S.; Salgado, J.; Ulrich, A. S. *Biophys. J.* **2009**, *96*, 3223−3232.
(24) Vostrikov, V. V.; Daily, A. E.; Greathouse, D. V.; Koeppe, R. E., II. *J. Biol. Chem.* **2010**, *285*, 31723−31730.
(25) Ladokhin, A. S.; Jayasinghe, S.; White, S. H. *Anal. Biochem.* **2000**, *285*, 235−245.
(26) Hall, B. A.; Chetwynd, A. P.; Sansom, M. S. P. *Biophys. J.* **2011**, *100*, 1940−1948.
(27) Monticelli, L.; Kandasamy, S. K.; Periole, X.; Larson, R. G.; Tieleman, D. P.; Marrink, S. J. *J. Chem. Theory Comput.* **2008**, *4*, 819−834.
(28) Stansfeld, P. J.; Sansom, M. S. P. *J. Chem. Theory Comput.* **2011**, *7*, 1157−1166.
(29) Strandberg, E.; Ozdirekcan, S.; Rijkers, D. T.; van der Wel, P. C.; Koeppe, R. E., II; Liskamp, R. M.; Killian, J. A. *Biophys. J.* **2004**, *86*, 3709−3721.
(30) Lewis, B. A.; Harbison, G. S.; Herzfeld, J.; Griffin, R. G. *Biochemistry* **1985**, *24*, 4671−4679.
(31) Cady, S. D.; Goodman, C.; Tatko, C. D.; DeGrado, W. F.; Hong, M. *J. Am. Chem. Soc.* **2007**, *129*, 5719−5729.
(32) Froyd-Rankenberg, J. M.; Greathouse, D. V.; Koeppe, R. E., II. *Biophys. J.* **2009**, *96*, 455a−456a.
(33) Killian, J. A.; Taylor, M. J.; Koeppe, R. E., II. *Biochemistry* **1992**, *31*, 11283−11290.
(34) Thomas, R.; Vostrikov, V. V.; Greathouse, D. V.; Koeppe, R. E., II. *Biochemistry* **2009**, *48*, 11883−11891.
(35) Lakowicz, J. R. *Principles of Fluorescence Spectroscopy*, 3rd ed.; Springer: New York, 2006.
(36) Koeppe, R. E., II; Killian, J. A.; Vogt, T. C. B.; De Kruijff, B.; Taylor, M. J.; Mattice, G. L.; Greathouse, D. V. *Biochemistry* **1995**, *34*, 9299−9306.
(37) Ottiger, M.; Bax, A. *J. Am. Chem. Soc.* **1998**, *120*, 12334−12341.
(38) Mittermaier, A.; Kay, L. E. *J. Am. Chem. Soc.* **1999**, *121*, 10608−10613.
(39) Sheppard, D.; Li, D. W.; Godoy-Ruiz, R.; Bruschweiler, R.; Tugarinov, V. *J. Am. Chem. Soc.* **2010**, *132*, 7709−7719.